Tellus (1995), 47A, 575–596
Printed in Belgium – all rights reserved

TELLUS
ISSN 0280–6495

Planetary and synoptic-scale interactions during the life cycle of a mid-latitude blocking anticyclone over the North Atlantic

By ANTHONY R. LUPO* and PHILLIP J. SMITH, *Department of Earth and Atmospheric Sciences, Purdue University, West Lafayette, IN 47907, USA*

(Manuscript received 29 August 1994; in final form 6 March 1995)

ABSTRACT

The formation of a blocking anticyclone over the North Atlantic has been examined over its entire life-cycle using the Zwack–Okossi (Z–O) equation as the diagnostic tool. This blocking anticyclone occurred in late October and early November of 1985. The data used were provided by the NASA Goddard Laboratory for Atmospheres on a global 2.0° latitude by 2.5° longitude grid. The horizontal distribution of the atmospheric forcing mechanisms that were important to 500 mb block formation, maintenance and decay were examined. A scale-partitioned form of the Z–O equation was then used to examine the relative importance of forcing on the planetary and synoptic scales, and their interactions. As seen in previous studies, the results presented here show that upper tropospheric anticyclonic vorticity advection was the most important contributor to block formation and maintenance. However, adiabatic warming, and vorticity tilting were also important at various times during the block lifetime. In association with precursor surface cyclogenesis, the 300 mb jet streak in the downstream (upstream) from a long-wave trough (ridge) amplified significantly. This strengthening of the jet streak enhanced the anticyclonic vorticity advection field that aided the amplification of a 500 mb short-wave ridge. The partitioned height tendency results demonstrate that the interactions between the planetary and synoptic-scale through vorticity advection was the most important contributor to block formation. Planetary-scale, synoptic-scale, and their interactions contributed weakly to the maintenance of the blocking anticyclone, with the advection of synoptic-scale vorticity by the planetary-scale flow playing a more important role. Planetary-scale decay of the long-wave ridge contributed to the demise of this blocking event.

1. Introduction

Blocking anticyclones are large-scale phenomena which can have profound impact on mid-latitude weather and climatic conditions not only over the regions in which they occur, but also over upstream and downstream areas as well (Rex, 1950, 1951; Illari, 1984; Agayan and Mokhov, 1989; Mokhov, 1993). The formation of blocking anticyclones has proven to be a difficult problem for both operational forecasting and for various forecast models (Simmons, 1986; Tibaldi and Molteni, 1990; Tracton, 1990; Tibaldi et al., 1993, 1994), even though their climatological behavior is well known (Rex, 1950; Triedl et al., 1981; Lejenas and Okland, 1983; Lupo and Smith, 1995). Many studies have shown the importance of large-scale forcing, such as long-wave baroclinic processes or topography, in block formation and maintenance (Charney and Devore, 1979; Sperenza, 1986; Dole, 1986). Other studies have described the configurations of and/or the interactions between long waves in blocked flows (Austin, 1980; Lejenas and Madden, 1992). In particular, a series of papers by Tung and Lindzen (1979) attempts to explain blocking as caused by the resonant amplification of large-scale planetary waves forced by those mechanisms named above. McWilliams (1980)

* Corresponding author.

demonstrates that blocking anticyclones have characteristics consistent with that of a solitary wave ("modon"), which in their simplest form consist of a high-low vortex pair. Modons are uniformly translating, shape preserving, non-linear analytic solutions of, in the case of the McWilliams study, the inviscid equivalent barotropic potential vorticity tendency equation. Frederiksen (1982) considers the problem of blocking as instabilities which grow in three-dimensional flows. He studied the problem using a variety of static stabilities corresponding to differing flow stabilities. All of these studies show plausible mechanisms for block formation and maintenance. However, they fail to address such issues as why blocks tend to occur in preferred geographic locations (Frederiksen, 1982), why blocks are observed to form and decay on time scales more consistent with synoptic-scale phenomena (Lupo and Smith, 1995), or why blocks are observed to "fluctuate" in intensity (or regenerate) during their life-cycle (McWilliams, 1980). More recently, another set of studies has demonstrated the importance of mid-latitude transients on block formation (Alberta et al., 1991; Colucci, 1985, 1987; Mullen, 1987; Shutts, 1983, 1986; Konrad and Colucci, 1988; Tsou and Smith, 1990; Tracton, 1990).

Diagnostic studies have utilized a variety of methods to examine the atmospheric forcing mechanisms that are important in block formation and maintenance. Hansen and Chen (1982) used atmospheric energetics equations in spectral space to examine both a Pacific and an Atlantic blocking case. They concluded that two processes that lead to block formation are the non-linear forcing of ultra long waves by intense cyclogenesis (mode 1 blocking), and the baroclinic amplification of planetary-scale waves (mode 2 blocking). Both scenarios were preceded by intense upstream surface cyclogenesis. Dole (1986) performed a composite analysis of persistent Pacific region positive (blocking anticyclones) and negative ("cutoff" lows) anomaly events to describe their vertical and thermal structures and their relationship to the zonal flow in the jet region. He found that during development both classes of anomalies exhibited a highly baroclinic structure and that formation and decay often occurred very rapidly. He also found that no regional atmospheric precursor was evident until just prior to development. Mullen (1987) used the quasi-geostrophic potential vorticity equation to examine the importance of synoptic-scale eddy forcing on composite (time mean) Atlantic and Pacific blocking flows. He found that eddy vorticity transports, occurring one-quarter wave length upstream from the blocking ridge, and eddy heat transports were important during development, but that the former was more important than the latter in maintaining the composite blocks. Also, he found that baroclinic instability was a very important mechanism in the formation of synoptic-scale eddies associated with blocking. Alberta et al. (1991), Tsou and Smith (1990), and Tracton (1990) used various forms of the height tendency equation, the vorticity equation, or the omega equation as their diagnostic tools. They all determined that anticyclonic vorticity advection was important in block formation. The first two studies also noted the importance of temperature advection in block formation, while Tracton (1990) found this mechanism played a more indirect role. Alberta et al. (1991) noted that once the block was established, barotropic forcing processes dominated the maintenance period. Alberta et al. (1991) and Tsou and Smith (1990) also found block formation to be preceded by a rapidly developing surface cyclone. Additionally, Tsou and Smith (1990) noted the importance of an associated jet streak just prior to block onset and just after the period of rapid surface cyclone development.

Since the studies mentioned above show blocking to involve both synoptic-scale and planetary-scale processes, some diagnostic studies have attempted to isolate the contributions of each and examine their interactions. Tsou and Smith (1990) use a partitioned form of the extended height tendency equation to examine the role each scale and their interactions play in block formation. They found that the interaction component, dominated by the advection of synoptic-scale vorticity by the planetary-scale winds, was the largest contributor to block formation. They also show that block formation is the result of the superposition of a mobile and amplifying synoptic-scale ridge and a large-scale stationary planetary-scale ridge. Following Tsou and Smith (1990), Tracton (1990) uses a spectral decomposition of 500 mb height fields to demonstrate that blocking reflects the superposition of synoptic-scale (and smaller scale) and planetary-scale wave modes. He used the

quasi-geostrophic vorticity and omega equations as the basic framework of his investigation and found results similar to the scale partitioned results of Tsou and Smith (1990).

Many of the studies mentioned above focus on the development of blocking anticyclones, and a few examine their maintenance. Only one of these studies (Dole, 1986) examines the decay period of blocking anticyclones. Considering the difficulty that forecast models encounter during block formation and decay (Tibaldi and Molteni, 1990; Tracton, 1990; Tibaldi et al., 1993, 1994), there is a clear need for more studies involving the entire life-cycle of blocking anticyclones (Tracton, 1990). In this paper, a diagnosis of the *entire* life-cycle of an individual 500 mb blocking anticyclone event is performed. Using the Zwack–Okossi equation (Zwack and Okossi, 1986; Lupo et al., 1992) as the primary diagnostic tool, the horizontal distribution of various atmospheric forcing mechanisms are studied. In addition, by partitioning the basic data into their planetary-scale and synoptic-scale components, the atmospheric forcing on each scale, as well as the interaction between the scales is also examined over the block life-cycle. Another unique aspect of this work is that a blocking anticyclone preceded by non-explosive cyclogenesis is examined. Previous studies similar to this one, notably Tsou and Smith (1990) and Tracton (1990), examine blocking anticyclones that were preceded by explosive cyclogenesis. Finally, the primary objective of this diagnosis is to elaborate on the Tsou and Smith (1990) block formation mechanism, with particular attention given to the role that the intervening jet streak plays in block formation.

2. Data

The data used in this investigation were analyses obtained from NASA/Goddard Laboratory for Atmospheres (GLA) (Schubert et al., 1993). This assimilated data set covers a 5-year period from 1 March 1985 through 28 February 1990. Analyzed fields were provided on a 2.0° latitude by 2.5° longitude grid at 14 mandatory pressure levels from 1000 to 20 mb at 6-h intervals for the entire globe. These fields include upper air parameters u and v (horizontal wind vector components in m/s), z (geopotential height (m)), T (absolute temperature), rh (relative humidity), and q (mixing ratio (g/kg)), all of which were then interpolated linearly in $\ln(p)$ to 50 mb isobaric levels. Also included were a variety of surface parameters; a complete list of these can be found in Schubert et al. (1993). The analysis scheme incorporated data from a variety of sources. The basic components of the assimilation system, model physics, and parameterizations used are described in more detail by Baker et al. (1987) and Schubert et al. (1993). Finally, subsets of these data are available upon further request from the Goddard Distributed Active Archive Center (DAAC). The subset of data utilized for this study covers the period from 26 October to 30 November 1985.

3. Computational procedures

The diagnosis was accomplished using the Zwack–Okossi (Z–O) equation (Zwack and Okossi, 1986) in its complete form (Lupo et al., 1992). The Z–O equation is a geostrophic vorticity tendency ($\partial\zeta_g/\partial t$) equation derived by coupling the vorticity and thermodynamic tendency equations through the hydrostatic thickness equation (Lupo et al., 1992). The result is a generalization of the Petterssen–Sutcliffe equation (Petterssen, 1956, p. 324) that allows for the diagnosis of geostrophic vorticity tendency at a near-surface pressure level as forced by dynamic and thermodynamic forcing mechanisms vertically integrated through the depth of the entire atmosphere.

To use the Z–O methodology for diagnoses at pressure levels aloft (pi), it is necessary to formulate a geostrophic vorticity tendency equation for level pi which includes the near-surface geostrophic vorticity tendency. This is easily accomplished by taking the horizontal laplacian and Eulerian time derivative of the hydrostatic thickness tendency equation, multiplying by the gravitational acceleration, and dividing by the Coriolis parameter (f) to yield the Z–O upper-air tendency equation:

$$\left.\frac{\partial\zeta_g}{\partial t}\right)_{pi} = \left.\frac{\partial\zeta_g}{\partial t}\right)_{p'} + \frac{R}{f}\int_{pi}^{p'} \nabla^2 \times\left(-\boldsymbol{V}\cdot\nabla T + \frac{\dot{Q}}{c_p} + S\omega\right)\frac{\mathrm{d}p}{p}, \qquad (1)$$

where, in this study, pi = 500 mb; pℓ represents a near-surface level (the first 50 mb pressure level above the earth's surface at any grid point); $\boldsymbol{V}$ is the horizontal wind vector; $\dot{Q}$ the diabatic heating rate; S the static stability parameter $(-T/\theta)(\partial\theta/\partial p)$; ω the vertical motion $(\mathrm{d}p/\mathrm{d}t)$; ∇ the del operator on an isobaric surface; and R, c_p, T, and θ, the gas constant for dry air, the specific heat at a constant pressure, absolute temperature, and potential temperature, respectively. The near-surface geostrophic vorticity tendency $(\partial\zeta_g/\partial t)_{p\ell}$ is then given by the complete Z–O near-surface tendency equation:

$$\left(\frac{\partial\zeta_g}{\partial t}\right)_{p\ell} = \mathrm{PD}\int_{p_t}^{p\ell}\Bigg(\underbrace{-\boldsymbol{V}\cdot\nabla\zeta_a}_{\text{(a) vadv}} \underbrace{-\omega\frac{\partial\zeta_a}{\partial p}}_{\text{(b) vvte}} \underbrace{+\zeta_a\frac{\partial\omega}{\partial p}}_{\text{(c) dive}}$$

$$\underbrace{-\hat{\boldsymbol{k}}\left(\nabla\omega\times\frac{\partial\boldsymbol{V}}{\partial p}\right)}_{\text{(d) tilt}} \underbrace{+\hat{\boldsymbol{k}}\cdot(\nabla\times\boldsymbol{F})}_{\text{(e) fric}} \underbrace{-\frac{\partial\zeta_{ag}}{\partial t}}_{\text{(f) ageo}}\Bigg)\mathrm{d}p$$

$$-\frac{(\mathrm{PD})\,R}{f}\int_{p_t}^{p\ell}\left[\int_{p}^{p\ell}\times\nabla^2\left(\underbrace{-\boldsymbol{V}\cdot\nabla T}_{\text{(g) tadv}}+\underbrace{\frac{\dot{Q}}{c_p}}_{\text{(h) diab}}+\underbrace{S\omega}_{\text{(i) adia}}\right)\frac{\mathrm{d}p}{p}\right]\mathrm{d}p. \qquad (2)$$

In (2), $\boldsymbol{F}$ is the frictional force, ζ_a the absolute vorticity, and ζ_{ag} the ageostrophic vorticity. Also, PD is $(1/(\mathrm{p}\ell - p_t))$, where p_t is the pressure at some sufficiently high pressure level (30 mb in this study) chosen to encompass most of the atmospheric mass. Forcing mechanisms (a) through (f) on the right-hand-side of (2) are the dynamic forcing mechanisms coming from the vorticity equation, while the remaining terms (g), (h), and (i) are the thermodynamic forcing mechanisms. Finally, (1) was relaxed to produce height tendencies at pi. These height tendencies were then filtered to remove all information below $5\Delta x$ (<1000 km), thus removing subsynoptic-scale noise present due to data, model, and computational errors.

In (1) and (2), ω was calculated using a complete form of the omega equation similar to that of Krishnamurti (1968):

$$\nabla^2\sigma\omega + f\zeta_a\frac{\partial^2\omega}{\partial p^2} = f\frac{\partial}{\partial p}\times\left(\boldsymbol{V}\cdot\nabla\zeta_a - \hat{\boldsymbol{k}}\cdot\nabla\times\boldsymbol{F} + \frac{\partial\boldsymbol{V}}{\partial p}\times\nabla\omega\right) + f\omega\frac{\partial^2\zeta}{\partial p^2} + \frac{R}{p}\nabla^2\left(\boldsymbol{V}\cdot\nabla T - \frac{\dot{Q}}{c_p}\right). \qquad (3)$$

In (1), (2), and (3) the frictional force was restricted to the boundary layer and was calculated using the Krishnamurti (1968) algorithm. Diabatic heating included convective and stable latent heat release (Fosdick and Smith, 1991; Lupo et al., 1992), boundary-layer sensible heating (Lupo et al., 1992), and a longwave radiation parameterization (Sasamori, 1968) that assumes randomly overlapped clouds (Harshvardhan et al., 1987). The boundary-layer sensible heating calculation included contributions from all isobaric levels between the near-surface level to the first isobaric level above the planetary boundary layer (PBL) as calculated by the Goddard Earth Observing System Atmospheric General Circulation Model (GEOS-1 AGCM). The long-wave radiation parameterization included contributions due to water vapor, carbon dioxide, and ozone. The ageostrophic vorticity tendency was calculated from the ageostrophic wind, which is turn was calculated as the vector difference between the observed and geostrophic wind. All horizontal (vertical) derivatives were calculated using 4th (2nd)-order finite differencing. Vertical integrals were calculated using the trapezoidal rule, and all relaxation was accomplished using sequential over-relaxation (SOR) (Haltiner and Williams, 1980, pp. 157–164).

All the computations described in this chapter were carried out over the entire Northern Hemisphere in order to reduce the influence of the boundaries in the central region of the grid. However, all comparisons between Z–O and observed height tendencies were made within a particular region. This region was chosen so as to encompass the blocking anticyclone and it's immediate vicinity in the upstream and downstream directions. For part of the life-cycle of the

block (prior to 1200 GMT 2 November), this region was bounded by 70° N, 30° N, 70° W, and 10° W. This area covered most of the North Atlantic, Eastern North America, Greenland, and Western Europe. The remaining part of the block life-cycle was examined in a region bounded by 70° N, 30° N, 90° W, and 30° W. This region covered the eastern third of North America and the Western North Atlantic. Comparisons were made using correlation coefficients between the Z–O equation height tendencies and observed ±6-h finite differenced height tendencies and mean absolute values of Z–O and observed tendencies, both over all grid points contained in the domains defined above.

A scale partitioning procedure following that of Tsou and Smith (1990) was employed to partition the basic data fields into their planetary-scale and synoptic scale components. The scale partitioning was accomplished using a second-order two-dimensional Shapiro (1970) filter applied 1250 times to the basic data fields. Applying the filter in this manner yields a response function (Fig. 1, curve a), which retains approximately 2%, 44%, and 80% of the signal for waves having a horizontal wavelength of 3000, 4500, and 6000 km at 45° N, respectively. This particular response function was chosen because blocking anticyclones typically have wavelengths of 6000 km. Also, since at 45° N 6000 km represents a hemispheric wave number between 4 and 5, the filtered data can be regarded as the planetary-scale component, and that part which was filtered out (the difference between the total and filtered component) becomes the synoptic-scale component. It should be noted here that the filtering procedure differs from that of Tsou and Smith (1990), who used a Barnes filtering procedure similar to Maddox (1980). While the filtering procedure was different in order to save computing time, the filtering parameters were chosen such that our response function (Fig. 1, curve a) was similar to that of Tsou and Smith (1990) (their Fig. 1).

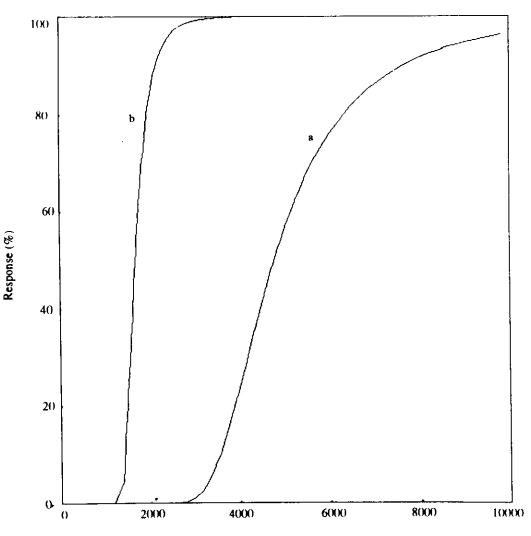

Fig. 1. Response curves for the (a) 2nd-order and (b) 4th-order 2-dimensional Shapiro (1970) filter.

As noted previously, height tendencies were filtered to remove small scale (<1000 km) noise without significantly degrading the large-scale information. This was accomplished using a 4th-order, 2-dimensional Shapiro filter applied 1250 times to all height tendencies. The response function for this filter is curve b in Fig. 1.

Finally, the filtered data fields were used in a partitioned form of the Z–O equation derived by substituting for each variable X:

$$X = \bar{X} + X', \tag{4}$$

where $\bar{X}(X')$ represents the planetary-scale (synoptic-scale) component. Using this technique in (1) yields an equation of the form:

$$\left.\frac{\partial \zeta_g}{\partial t}\right]_{pi} = P + S + I, \tag{5}$$

where P, S, and I represent the planetary-scale, synoptic-scale, and scale-interaction components, respectively, of the forcing processes on the right-hand-side. A similar equation for $\partial\zeta_g/\partial t]_{p\ell}$ occurs when the terms in (2) are partitioned. An example of the result of this process as applied to term (a) on the right-hand-side of (2), or the contribution to the total tendency by vorticity advection, in both (1) and (2), is:

$$\left.\left(\frac{\partial \zeta_g}{\partial t}\right)_{p\ell}\right]_{vadv} = PD \int_{p_t}^{p\ell} (\underbrace{-\bar{V}\cdot\nabla\bar{\zeta}_a}_{P} \underbrace{-V'\cdot\nabla\zeta'_a}_{S} \underbrace{-\bar{V}\cdot\nabla\zeta'_a}_{I_1} \underbrace{-V'\cdot\nabla\bar{\zeta}_a}_{I_2})\, dp, \tag{6}$$

where I_1 is the advection of synoptic-scale vorticity by the planetary-scale wind, I_2 is the advection of planetary-scale vorticity by the synoptic-scale wind, and $I_1 + I_2 = I$.

4. Synoptic discussion

Fig. 2 is a graph of 500 mb central or maximum height values spanning the pre-block 500 mb ridge and blocking anticyclone period. Significant dates and periods within the blocking anticyclone's life cycle are labeled on the x-axis or defined inside the figure. The procedures for choosing the central or maximum height values and time of block onset and termination are specified in Lupo and Smith (1995). In addition, the synoptic discussion that follows is based on the dates in Fig. 2. The pre-development 500 mb Atlantic region environment, represented by 1200 GMT 28 October 1985, shows a long-wave trough located over the western North Atlantic, eastern Canada, and the north-eastern United States (Fig. 3a). Embedded within this trough was a closed cyclone located over the Gulf of St. Lawrence (48° N, 65° W) and a short-wave ridge to the east of the closed center and south of Greenland. A stationary long-wave ridge was located over the eastern Atlantic and much of Europe. A surface cyclone located over Newfoundland had reached the end of its development phase with a central pressure of 990 mb.

By 1800 GMT 29 October (Fig. 3c), the 500 mb low was located over Newfoundland and had reached its minimum height 6-h earlier. The short-wave ridge, now located over southern Greenland and extending approximately 500 km into the North Atlantic, had propagated northeastward with a northwest-to-southeast oriented axis. This ridge became stationary at this time. Also, at this time a cyclonically curved jet streak at 300 mb was located along 50° W on the eastern (western) flank of the long-wave trough (ridge) (Fig. 3d). The surface cyclone noted above, with nearly the same central pressure, had moved northwestward slightly such that by this time there was little tilt with height. After this time the cyclone decayed rapidly and disappeared 12-h later. A second surface cyclone was just forming along a surface trough extending southward from the first low. This second cyclone first appeared as a closed system at this time with a central pressure of 996 mb at 42° N, 50° W, or 700 km southeast of Newfoundland (Fig. 3b), and is of special interest because it is the precursor cyclone to the block development. References to a surface cyclone and cyclogenesis in the next two paragraphs apply to this cyclone.

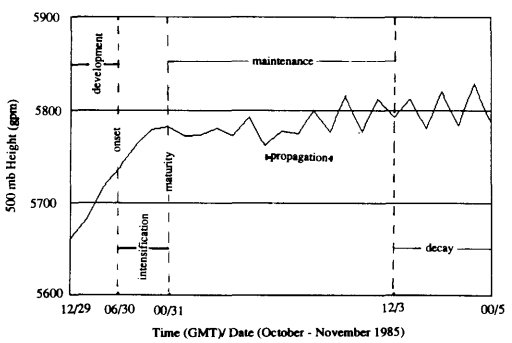

Fig. 2. Plot of 500 mb maximum or central height values (gpm) for the 500 mb short-wave ridge or blocking anticyclone versus time. Important periods of time within the block's lifecycle are separated by the vertical dashed lines.

By 0600 GMT 30 October (Fig. 3e), the 500 mb short-wave ridge had intensified and a closed anticyclone center appeared southeast of Greenland (56° N, 32.5° W), indicative of block onset. Also a closed high pressure area at the surface (not shown) appeared in approximately the same locale with a central pressure of 1026 mb. This surface anticyclone could be identified with the 500 mb anticyclone throughout the block lifetime. The 300 mb jet streak (Fig. 3f) had also intensified with the maximum wind speeds increasing approximately 25% in the first 12-h, 80% of which occurred in the first 6-h, following the start of surface cyclogenesis (1800 GMT 29 October). The short-wave amplification and intensifying jet streak upstream of the closed anticyclone, the latter associated with the developing surface cyclone, is a block development scenario similar to the conceptual model proposed by Tsou and Smith (1990).

The blocking anticyclone remained nearly stationary for 42-h after onset. During this period it intensified most rapidly, reaching maturity at 0000 GMT 31 October (Fig. 3g). At block onset, the surface cyclone was midway through its period of most rapid deepening and had achieved a central pressure of 991 mb. Slower deepening occurred over the next 12-h and the cyclone

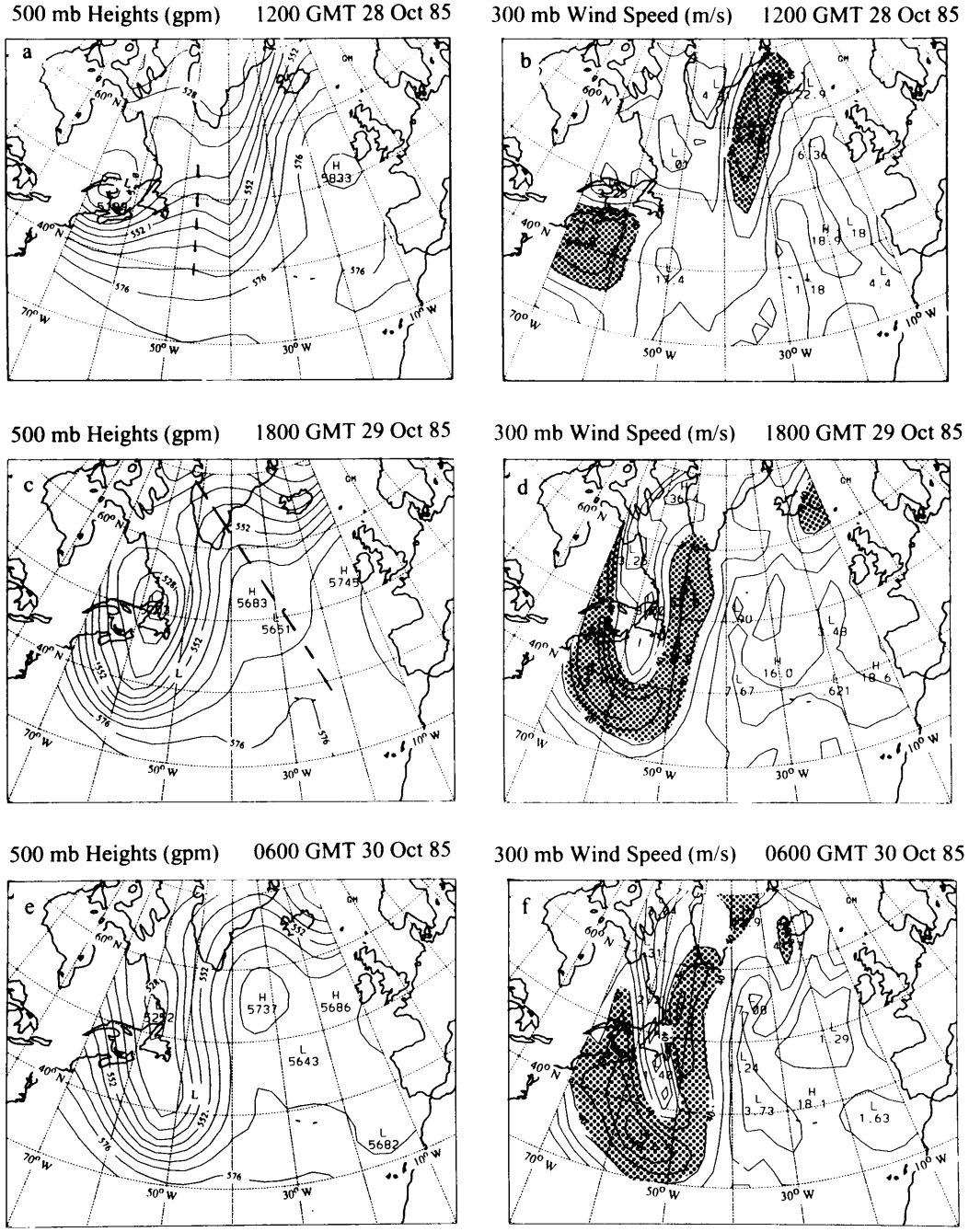

Fig. 3. Regional 500 mb height (gpm) and 300 mb windspeed ($m\ s^{-1}$) maps for (a) and (b) 1200 GMT 28 October, (c) and (d) 1800 GMT 29 October, (e) and (f) 0600 GMT 30 October, (g) and (h) 0000 GMT 31 October, (i) and (j) 1200 GMT 01 November, and (k) and (l) 1200 GMT 04 November 1985. The contour intervals are 60 gpm for the height fields and 10 ($m\ s^{-1}$) for the wind speeds. The surface cyclones are denoted by an "L" on the height maps. The shaded regions are wind speeds exceeding 40 ($m\ s^{-1}$).

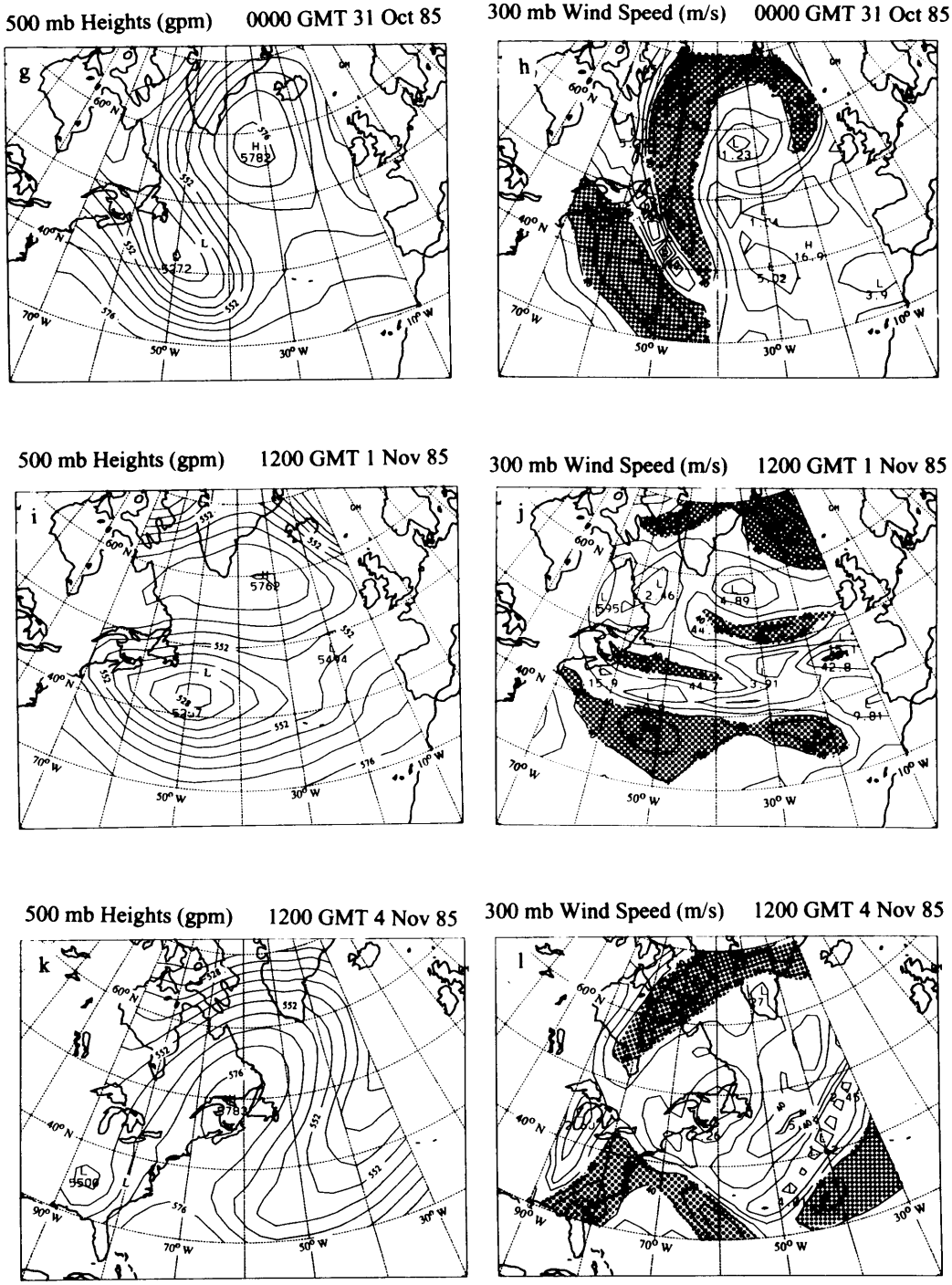
500 mb Heights (gpm) 0000 GMT 31 Oct 85
300 mb Wind Speed (m/s) 0000 GMT 31 Oct 85
500 mb Heights (gpm) 1200 GMT 1 Nov 85
300 mb Wind Speed (m/s) 1200 GMT 1 Nov 85
500 mb Heights (gpm) 1200 GMT 4 Nov 85
300 mb Wind Speed (m/s) 1200 GMT 4 Nov 85

Fig. 3. (cont'd).

attained its lowest central pressure of 988 mb at 1800 GMT 30 October (not shown). Throughout the remainder of the block lifetime, the occluded surface cyclone changed little in intensity and became associated with a 500 mb low that was part of the blocking dipole that was forming at 0000 GMT 31 October and is quite evident at 1200 GMT 01 November (Fig. 3i).

From 1200 GMT 1 November (Fig. 3i) through 1200 GMT 2 November (not shown), the blocking anticyclone propagated westward across the North Atlantic and into extreme eastern Canada (58° N, 62.5° W). During the 60-h period ending with 1200 GMT 2 November, the central height values of the blocking anticyclone remained nearly constant (Fig. 2). A strong anticyclonically curved jet nearly encircled the 500 mb anticyclone, such that a strong easterly jet streak was located between the 500 mb anticyclone/cyclone dipole (Fig. 3j). After 1200 GMT 2 November, the block again became nearly stationary and remained so for the balance of its lifetime. The surface anticyclone associated with the block had slowly intensified reaching a maximum of 1037 mb by this time.

The decay began after 1200 GMT 3 November (represented by Fig. 3k, 1200 GMT 4 November) and was characterized by the center of the anticyclone moving southward and the block losing its identity until it failed to meet the blocking criteria defined by Lupo and Smith (1995) on 0000 GMT 5 November. Note from Fig. 2 that the block decay is not marked by a decrease in central height values. During the 36-h period preceding 1200 GMT 3 November, the block underwent modest intensification (Fig. 2). After this time, the 500 mb cyclone that was part of the dipole became an open wave again as it moved east of the blocking ridge (see Fig. 3k). In addition, another surface cyclone, located over the southeast Atlantic coast of the United States, developed in association with an advancing upper air trough. During this development, the surface cyclone was located under a large region of 300 mb diffluent flow with jet maxima aligned in a configuration similar to that shown by Rodgers and Bosart (1991) (Fig. 3l). Therefore, unlike the configuration at block onset, and unlike the conceptual model of Tsou and Smith (1990), no jet streak was located on the eastern(western) flank of the 500 mb trough(ridge).

5. Results

5.1. Z–O diagnostic results

To conserve space, the ensuing discussion will focus on the results for map times *representative* of the block development (pre-block), intensification, maintenance, and decay periods, even though all 6-h time periods during the block lifetime were examined. Presented are total calculated 500 mb height tendencies and the contributions to the total height tendency by vorticity advection, temperature advection, and adiabatic temperature change (map depictions). These mechanisms were chosen because they were consistently the largest contributors to the total tendency in the region studied. Also shown are the contribution of the individual forcing terms at the center point (the maximum 500 mb height value) of the 500 mb anticyclone (bar graphs), which is denoted by an "X" in each map. The bar graphs were used to represent the development component of the height tendency, since at the center point the propagation component is zero. Comparison of the calculated 500 mb height tendencies with the centered ($\pm$6-h) finite difference height changes for each map time resulted in average correlation coefficients of 0.794 and mean absolute values for the two fields of 0.874×10^{-3} (gpm/s) and 1.029×10^{-3} (gpm/s), respectively. Thus, the calculated fields are reasonable representations of the observed height changes.

Using 0000 GMT 30 October to represent the block development period, Fig. 4a shows that the region of ridge amplification east and southeast of Greenland was experiencing height increases, while height falls were prominent over the region of the precursor cyclone. From Figs. 4b, e it is seen that anticyclonic vorticity advection (AVA) was the primary contributor to ridge amplification at 500 mb and had a spatial pattern similar to that of the total height tendency. The adiabatic temperature change also made a contribution to ridge amplification (Figs. 4d, e). The height rise maximum due to this term was located just slightly northeast of the ridge axis (see Figs. 3c, e). This maximum was due to a broad area of downward motion, whose profile (not shown) exhibited a maximum between 850 and 700 mb. The temperature advection term, like the remaining terms at the center point, was small (Figs. 4c, e). The other dynamic terms, with the exception of the

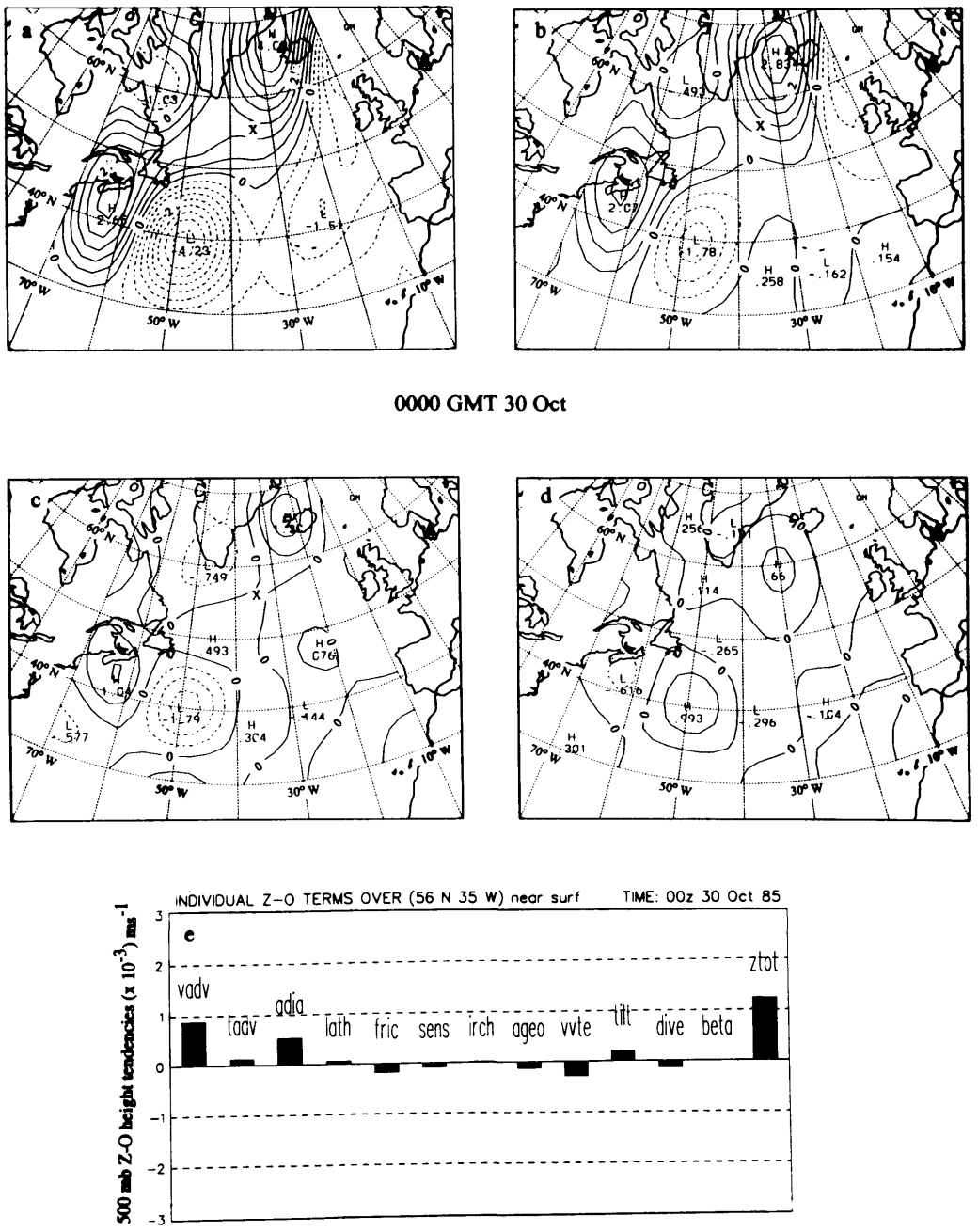

Fig. 4. (a) Regional 500 mb calculated height tendency fields, and (b), (c), and (d) are the contribution to the total tendency by vorticity advection, temperature advection, and adiabatic temperature change, respectively, for 0000 GMT 30 October 1985. (e) Bar graphs showing the contribution of each individual forcing term to the total tendency at the block center marked with an "X" in (a), (b), (c) and (d). Contour interval: 0.5 units. Units: 10^{-3} gpm s^{-1}.

vorticity tilting term, contributed to height falls along the ridge axis.

An examination of the 300 mb wind field (Figs. 3b, c, d) reveals that the ridge axis was located on the anticyclonic shear side of the 300 mb jet maximum. Also, the jet maximum itself strengthened considerably in association with the low-level cyclogenesis. This jet maximum also changed in shape such that the curvature changed from cyclonic to anticyclonic during block development in response to changes in the shape of the height field. Therefore, it is likely that the strong anticyclonic vorticity advection found along the ridge axis throughout the development period was due to both the anticyclonic curvature and shear components of the vorticity field. This region of anticyclonic vorticity advection increased in strength throughout the development period coinciding with the strengthening of the jet maximum discussed in Section 4. Thus, it is likely that baroclinic processes, such as temperature advection and latent heating played an indirect role in block formation the block by contributing to a strengthening of the jet maximum. This result and conclusion was also found by Tracton (1990).

The blocking anticyclone intensification period is represented by 1200 GMT 30 October. At this time, 500 mb height rise maxima were located northeast and west of the block center (Fig. 5a). Height rises over the block center had begun to diminish as had the forcing by each contributing term on the right-hand-side of (1) (Fig. 5e). By examining Figs. 5b, d, however, it is apparent that the height rise maxima induced by vorticity advection and adiabatic temperature change were no longer in close proximity to the block center as had been the case 12-h earlier. Fig. 5e shows that AVA, temperature advection, adiabatic temperature change, and vorticity tilting contributed to block intensification, while all the other terms inhibited intensification over the block center.

1200 GMT 1 November is representative of the 500 mb height tendencies during the block maintenance period. Fig. 6a shows that the height tendencies at the block center were generally weaker than at previous times, and the anticyclone center was near the zero tendency isopleth. Figs. 6b, c, and d also show that the forcing due to each mechanism was not necessarily weaker in the region. Rather, like the total tendency, the block center was located close to the zero isopleth in each field. Therefore, during this period, the total forcing and the forcing contributions from each individual term at the block center were very weak,with no one term consistently dominating the others (Fig. 6e). The total tendency at this particular time exhibits height falls, but this reflects the minor oscillations (as seen in Fig. 2) of the zero-tendency line relative to the block center that prevailed throughout the maintenance period. Additionally, it was during the maintenance period and after 1200 GMT 1 November that the block had moved westward, presumably encouraged by the height rise region west of the block.

The decay of the blocking anticyclone, represented by 1200 GMT 4 November, was marked by slow southward propagation of the center and the encroachment of height falls on the western flank and center of the block (Fig. 7a). The height fall maximum southwest of the block was associated with the advancing upper air trough mentioned previously. This height fall region was dominated by cyclonic vorticity advection, warm air advection (Figs. 7b, c), and latent heat release (not shown). From Figs. 7b, d, e, it can be seen that AVA, adiabatic warming, and vorticity tilting were still contributing to height rises at the block center at 500 mb, and prominent height rise maxima were located south-southwest of the block. However, a deep layer of upper tropospheric warm air advection associated with the advancing trough contributed significantly to height falls at this time. Combined with the negative contributions from all the other dynamic forcing terms, this was sufficient to produce 500 mb height falls over the block center.

5.2. *Scale-partitioned results*

An overview of the scale-partitioned results will, again for brevity, apply to the four representative map times used in Subsection 5.1. In addition, a detailed discussion of the results is restricted to total partitioned 500 mb height tendency fields and anticyclone center statistics in order to focus on the influence of the partitioned forcing terms on block development. An overall comparison of the P, S, and I term contributions can be obtained from the absolute values of the partitioned height tendencies averaged over the region presented in Table 1. These reveal that the planetary/synoptic-scale interaction height tendencies (I) and the syn-

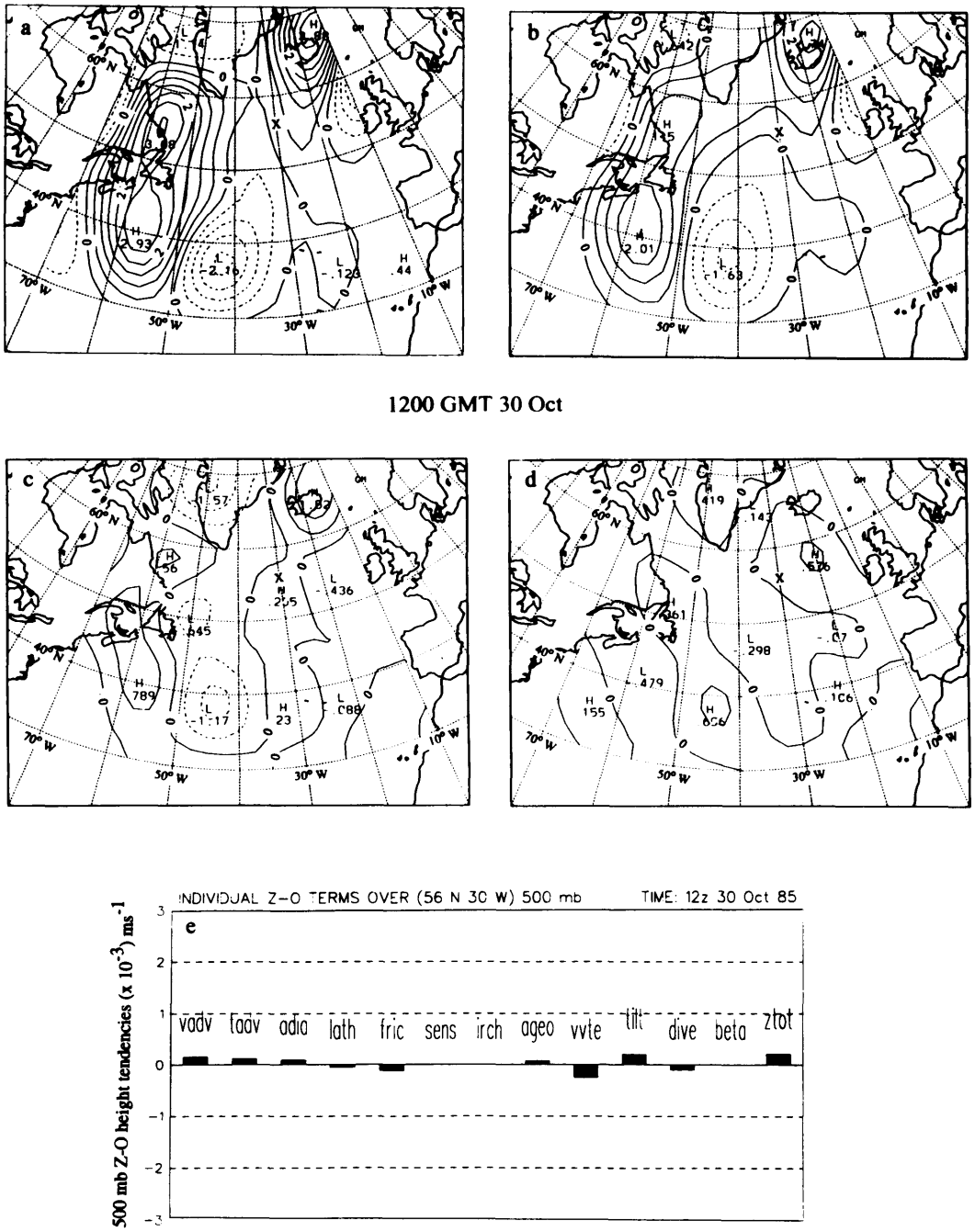

Fig. 5. As in Fig. 4 except for 1200 GMT 30 October 1985.

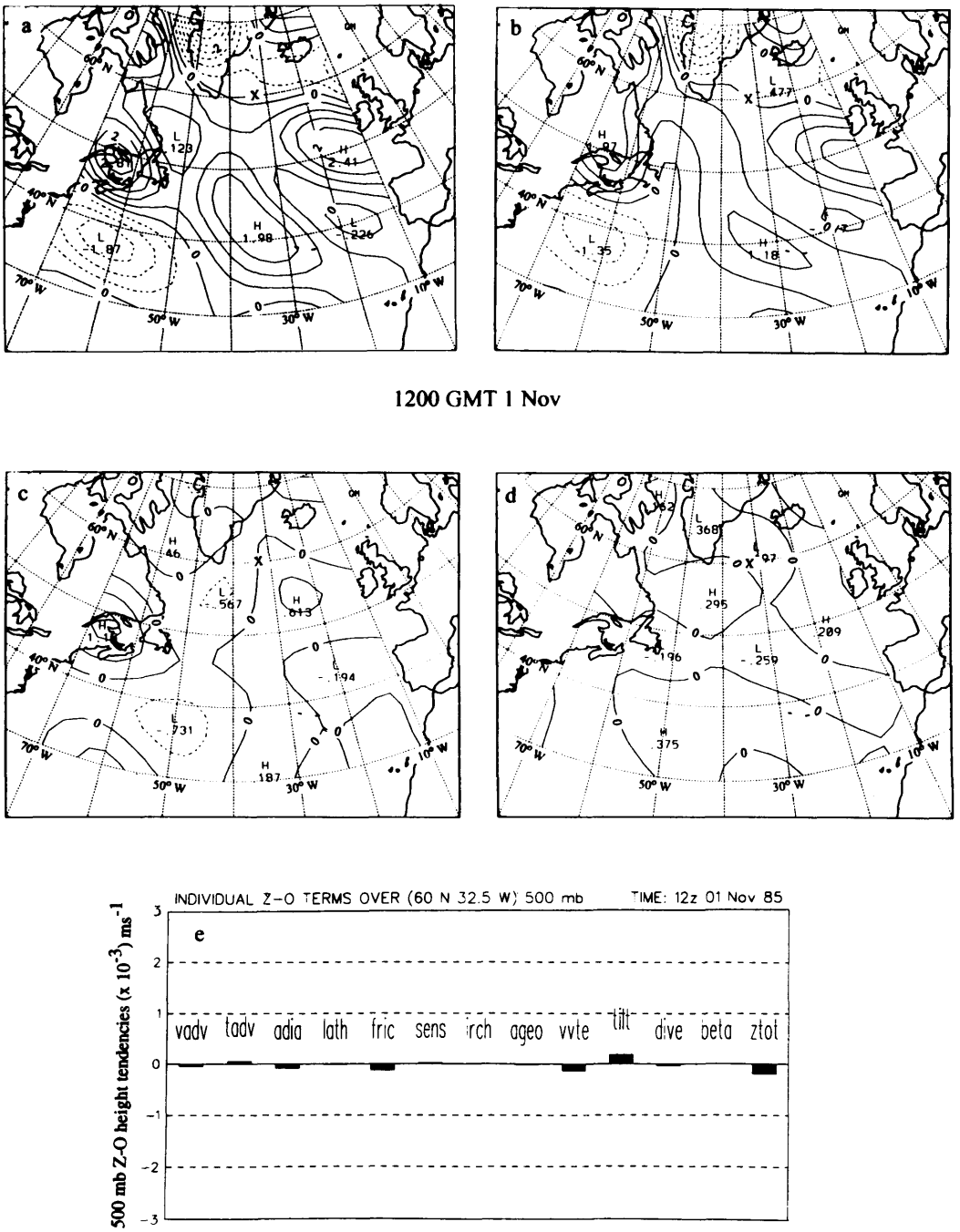

Fig. 6. As in Fig. 4 except for 1200 GMT 01 October 1985.

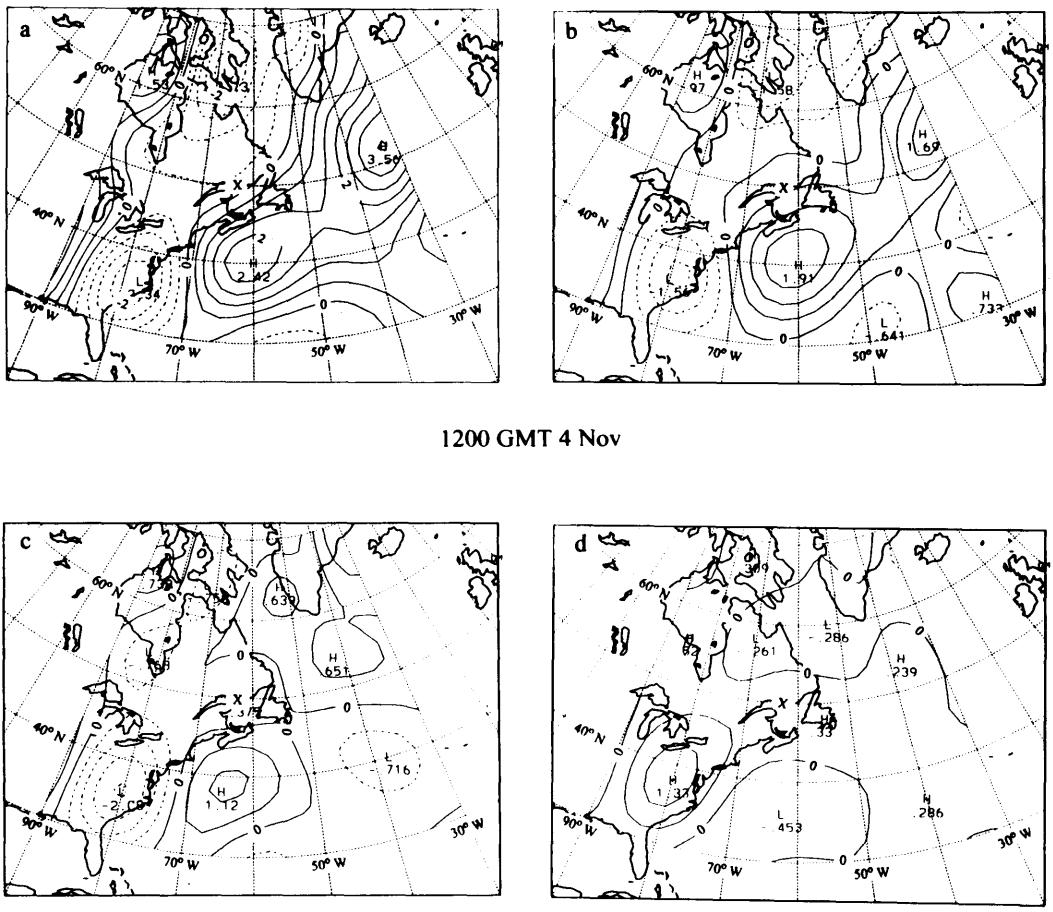

Fig. 7. As in Fig. 4 except for 1200 GMT 04 November 1985.

Table 1. *Mean absolute values of the regional partitioned height tendency (10^{-3} gpm/s) for (a) the first three periods and (b) the decay period of the block*

Scale \ Time period:	(a)	(b)
planetary (P)	0.1573	0.4475
synoptic (S)	0.4924	0.5449
interactions (I)	0.4899	0.6110

optic-scale height tendencies (S) were, on average, significantly larger than the planetary scale (P) height tendencies over the first three periods in the life cycle of the blocking event. While the I and S height tendencies were approximately equal in magnitude over these periods, the P height tendencies were only about one-third of the other two components, a result similar to that of Tsou and Smith (1990). Tracton (1990) found that the interaction component (I) was the dominant component in his case study. During the decay period, the

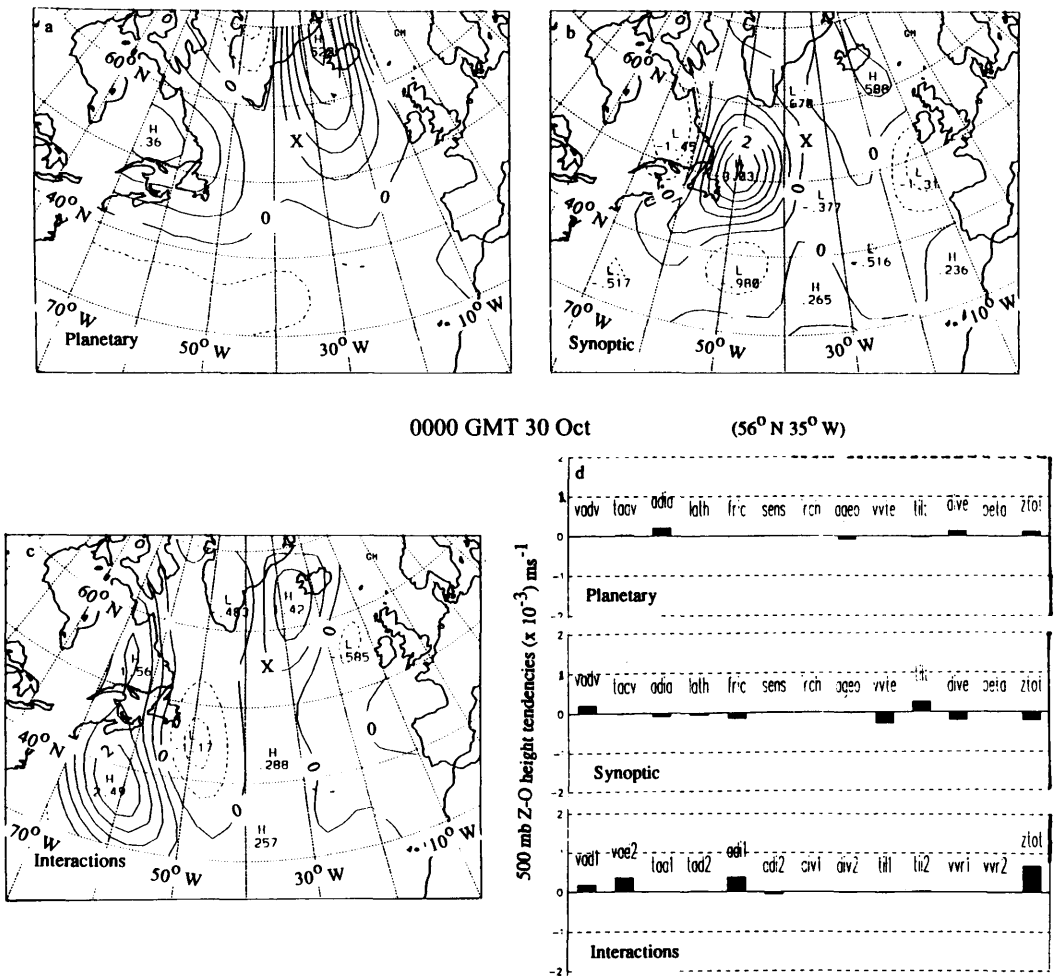

Fig. 8. Height tendency contributions to the Z–O total height tendency by the (a) planetary-scale, (b) synoptic-scale, and (c) planetary/synoptic-scale interaction components. (d) Bar graphs showing the contibution to the total tendency by each term at the block center point (X) on 0000 GMT 30 October 1985. Contour intervals: (a) 0.1 units and (b) and (c) 0.5 units. Units: 10^{-3} gpm s^{-1}.

Tellus A/47/5:1-5

Table 2. *Abbreviations of the forcing processes represented in the interaction height tendencies figures*

Vad1	$-\bar{V}\cdot\nabla\zeta'$	advection of synoptic-scale vorticity by the planetary-scale wind
Vad2	$-V'\cdot\nabla\bar{\zeta}$	advection of planetary-scale vorticity by the synoptic-scale wind
Tad1	$-\bar{V}\cdot\nabla T'$	advection of synoptic-scale temperature by the planetary-scale wind
Tad2	$-V'\cdot\nabla\bar{T}$	advection of planetary-scale temperature by the synoptic-scale wind
Adi1	$\bar{S}\omega'$	synoptic-scale vertical motion acting on the planetary-scale static stability field
Adi2	$S'\bar{\omega}$	planetary-scale vertical motion acting on the synoptic-scale static stability field
Div1	$\bar{\zeta}\frac{\partial\omega'}{\partial p}$	synoptic-scale divergence field interacting with the planetary-scale vorticity field
Div2	$\zeta'\frac{\partial\bar{\omega}}{\partial p}$	planetary-scale divergence field interacting with the synoptic-scale vorticity field
Til1	$-\frac{\partial\bar{V}}{\partial p}\times\nabla\omega'$	the cross product of the vertical shear of the planetary-scale wind and the gradient of the synoptic-scale vertical motion
Til2	$-\frac{\partial V}{\partial p}\times\nabla\bar{\omega}$	the cross product of the vertical shear of the synoptic-scale wind and the gradient of the planetary-scale vertical motion
Vvr1	$-\omega'\frac{\partial\bar{\zeta}}{\partial p}$	the advection of planetary-scale vorticity by the synoptic-scale vertical motion field
Vvr2	$-\bar{\omega}\frac{\partial\zeta'}{\partial p}$	the advection of synoptic-scale vorticity by the planetary-scale vertical motion field

magnitude of the I and S terms remained nearly the same. However, the magnitude of the P component increased to a value that was nearly equal in magnitude to the other two components.

The development period was dominated by 500 mb height rises over the amplifying small scale ridge (see Fig. 4), forced primarily by the interaction height rises (Fig. 8c). An area of planetary-scale height rises (Fig. 8a) is located nearly coincident with the interaction height rises, while a synoptic-scale height rise maximum (Fig. 8b) is located west of the block center. An examination of the individual contributors (Fig. 8d) to height rises shows that the vorticity advection term, which dominated development, was forced by the S and both terms in the I vorticity advections. It should be noted here that Table 2 describes the abbreviations found in Figs. 8d, 9d, 10d, and 11d. A comparison with earlier map times (not shown) reveals that it was the increase in amplitude of the interaction component that accounted for the increase in vorticity advection associated with the strengthening of the jet as discussed in Sections 4 and 5.1. The height rises due to adiabatic warming noted in Subsection 5.1 were contributed mainly by P and I. The I contribution was mostly due to vertical motion on the synoptic-scale interacting with the planetary-scale static stability field.

The intensification period, in general, was characterized by smaller 500 mb height rises over the center of the block (see Fig. 5). The I height rise component, due mainly to the advection of synoptic-scale vorticity by the planetary-scale wind, was again the main contributor to the height rises (Fig. 9d). This period was also characterized by a lack of significant contributions from the thermodynamic forcing mechanisms (Fig. 9d). The remaining dynamic forcing mechanisms were largely due to synoptic-scale processes. As in Fig. 5, it can be shown by examining Figs. 8a–c that the height rise maxima were not weaker than they were during development. These maxima, in particular the interaction and planetary-scale component maxima, were just located farther from the block center than they were 12-h earlier.

As discussed in Subsection 5.1, the maintenance period was marked by small 500 mb total tendencies and small contributions by each forcing mechanism. As was shown in Fig. 6, the block center was close to the zero tendency line for both the total height tendency and individual forcing tendencies. For most terms, the total parti-

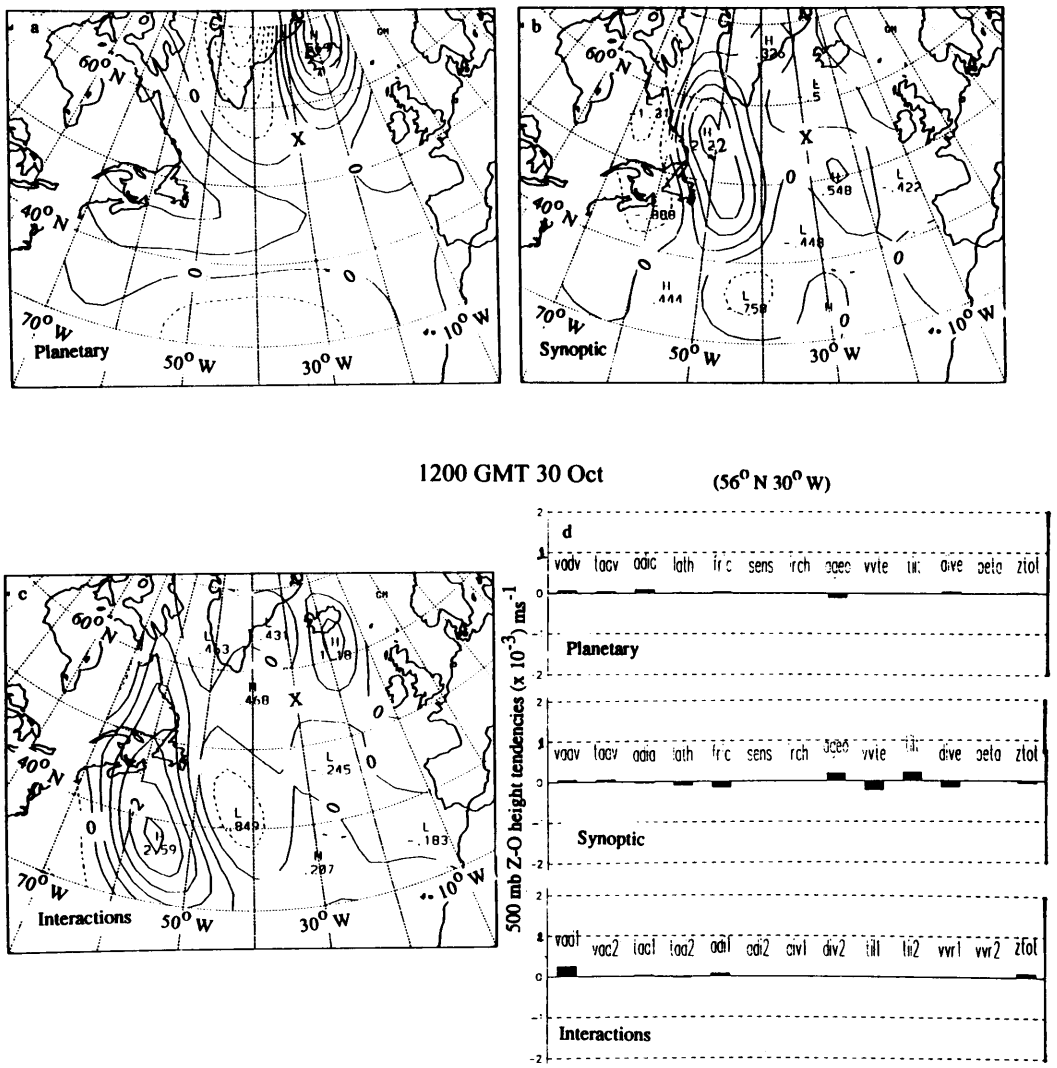

Fig. 9. As in Fig. 8 except for 1200 GMT 30 October 1985.

tioned height tendencies also reflected this trend (Figs. 10a–c). However, the important role of the synoptic-scale vorticity advection by the planetary-scale wind in maintaining the block is still evident (Fig. 10d).

In the decay period, the largest net height falls near and over the block center were contributed by the P terms (Fig. 11). At this time, AVA was still contributing to height rises over the block center; but, on the planetary-scale, cyclonic vorticity advection (CVA) was the largest contributor to height falls. All of the other P forcing processes, with the exception of adiabatic temperature change, were also producing height falls. In addition, most of the S and I terms were also forcing height falls. The warm air advection contributing

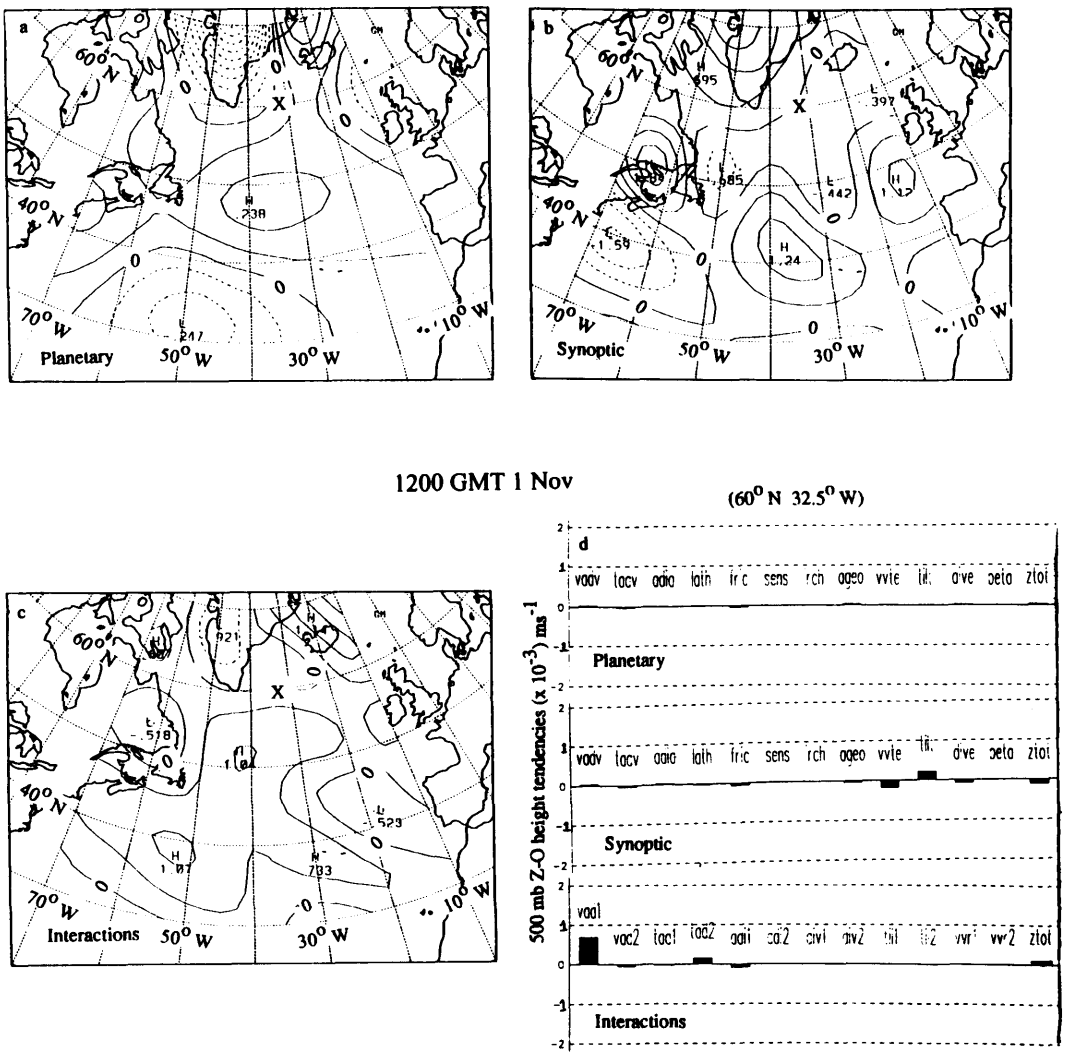

Fig. 10. As in Fig. 8 except for 1200 GMT 01 November 1985.

to height falls in Fig. 7e was comprised mainly of the interaction advections (Fig. 11d), while the dynamic mechanisms were mainly due to synoptic-scale processes.

Throughout the block life-cycle, the interaction component, which is clearly dominated by the advection of synoptic-scale vorticity by the planetary-scale wind (not shown), most resembles the total height tendency. This qualitative observation agrees with the findings of Tracton (1990) who found a high correlation between the advection of synoptic-scale vorticity by the planetary-scale wind and the total vorticity tendency. Additionally, the 300 mb wind field can be partitioned into a planetary-scale and synoptic-scale components (Fig. 12). Correlating each component of

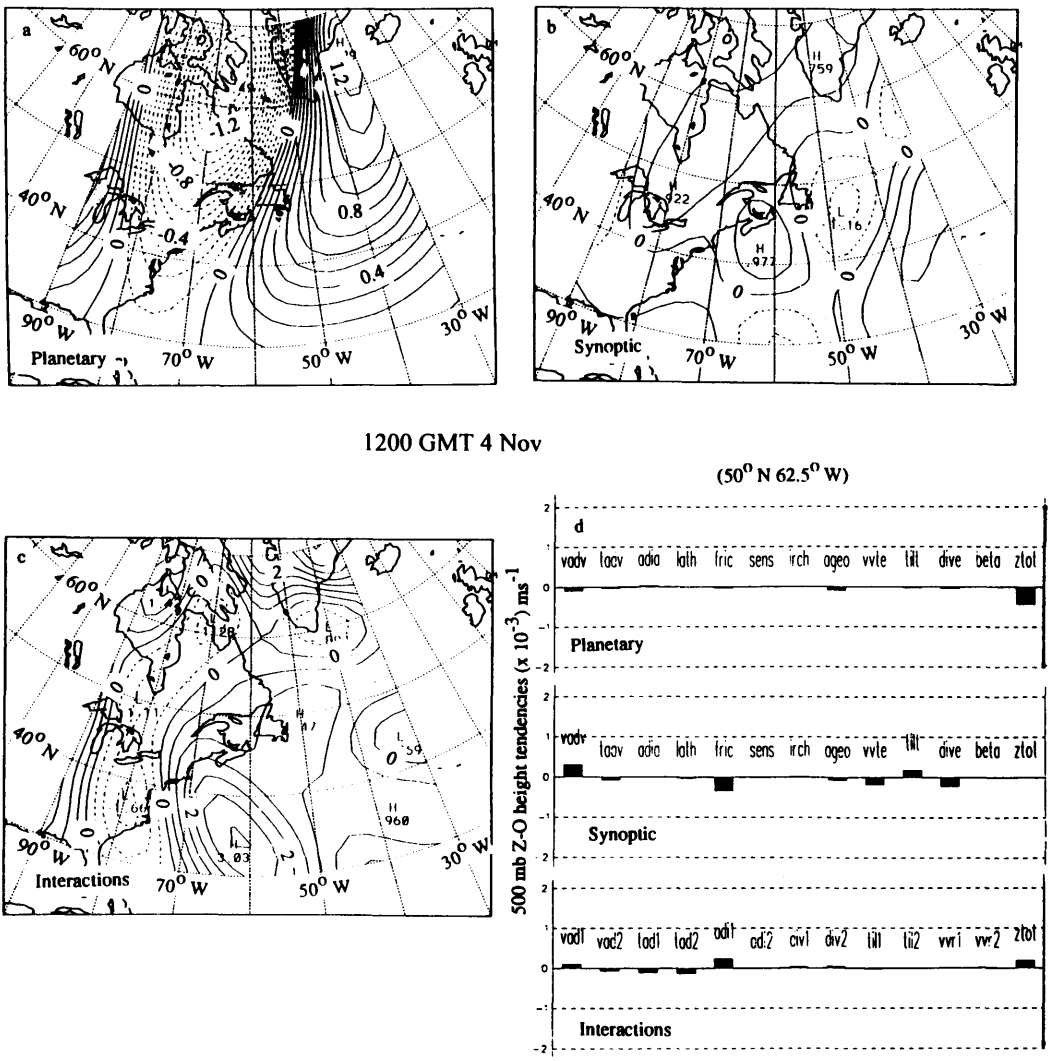

Fig. 11. As in Fig. 8 except for 1200 GMT 04 November 1985.

the wind field with each of the total partitioned tendencies reveals that the highest correlations were consistently between the synoptic-scale component of the total wind and the total interaction height tendencies (see Fig. 12). The correlations averaged 0.31 and ranged from 0.25–0.40. The other comparisons yielded correlations between −0.1 and 0.1. Note in the example of Fig. 12 that the interaction height rise regions are located close to the synoptic-scale jet maxima.

6. Conclusions

The formation of a blocking anticyclone over the North Atlantic Ocean during the fall of 1985 has been examined over its entire life cycle using the Z–O equation as the primary diagnostic tool and the Tsou and Smith (1990) block formation model as a guide. Similar diagnoses (Tsou and Smith, 1990; Tracton, 1990) have examined blocking anticyclones that were preceded by explosive

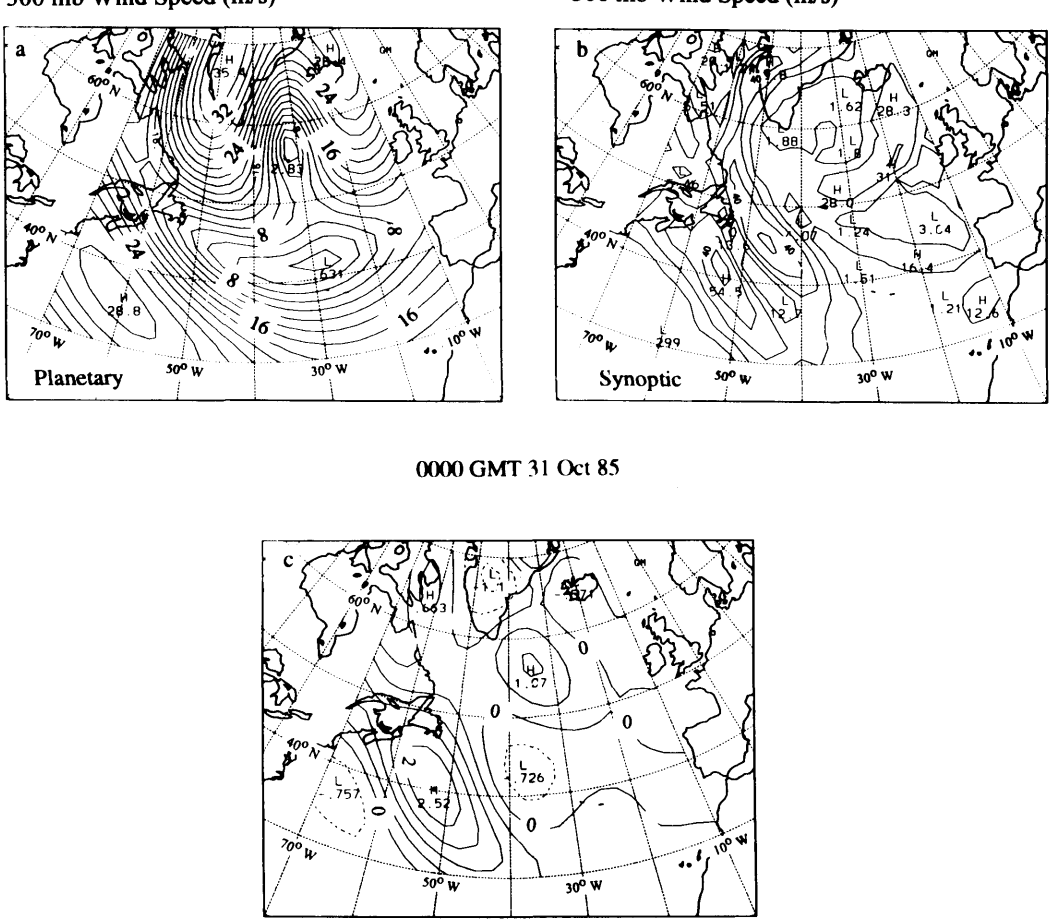

Fig. 12. The (a) planetary-scale and (b) synoptic-scale component of the 300 mb wind speeds ($m\,s^{-1}$) and (c) planetary/synoptic-scale interaction component of the total height tendencies ($\times 10^{-3}$ gpm s^{-1}) for 0000 GMT 31 October 1985. Contour intervals are: (a) 2, (b) 10, and (c) 0.5 units, respectively.

cyclones. This paper examines a blocking anticyclone preceded by a non-explosively developing cyclone and, unlike other studies, examines the entire block life-cycle. This paper, like many others, demonstrates the importance of mid-latitude transients, especially extratropical cyclones, in block formation and maintenance. Furthermore, as Dole (1986) found with Pacific positive and negative anomalies, this blocking anticyclone decayed just as rapidly as it developed, or on a time scale more consistent with synoptic-scale phenomena. Interestingly, in the case studied here, decay of the blocking anticyclone was also associated with an upstream developing cyclone. However, this cyclone was not accompanied by a jet streak favorably positioned as was the case for block development. More case studies are being examined to determine if this result can be found in other blocking anticyclones.

The relationship between blocks and jet streaks following the results of Tsou and Smith (1990), in which it is suggested that intervening jet streaks may play a role in the link between precursor cyclones and blocking anticyclones. In particular, the jet streak involved in this blocking anticyclone strengthened significantly in association with

surface cyclogenesis. The increased anticyclonic shear and curvature in turn strengthened the anticyclonic vorticity advection field that dominated the amplification of the downstream short-wave ridge. The location of jet streaks relative to the block center within the large-scale flow appeared to be important throughout the block life-cycle. As long as the jet maxima were located favorably, as in Tsou and Smith (1990), the block developed and was maintained. However, when they were located in an unfavorable configuration, or one favorable to cyclogenesis as in Rodgers and Bosart (1991), the block decayed.

In this diagnosis, it was found that anticyclonic vorticity advection was the largest contributor to block formation and maintenance at 500 mb. During much of the block life-cycle adiabatic warming resulting from downward motion, maximizing between 850 mb and 600 mb, and vorticity tilting also contributed to 500 mb height rises over the anticyclone center. The other thermodynamic mechanisms were very small until the decay period, when temperature advection contributed to height falls and the other dynamic forcing mechanisms also contributed to height falls over the block center. The block decayed when forcing processes contributing to height falls overwhelmed those contributing to height rises.

The partitioned height tendencies over the anticyclone center demonstrated that the interaction component, largely due to the advection of synoptic-scale vorticity by the planetary-scale wind, dominated the total height tendency from development through maintenance. The adiabatic warming that contributed to block formation and maintenance described in Subsection 5.1, was dominated by the synoptic-scale vertical motion acting on the planetary-scale static stability field. During maintenance, the S and I components were jointly responsible for the height rise region west of the block, and this region probably encouraged the westward propagation ending at 1200 GMT 02 November 1985. During decay the planetary-scale forcing assumed a greater role in contributing to the total height tendency field. The regional MAVs showed that the synoptic-scale and interaction components were nearly of equal magnitude throughout the block life-cycle. This result was similar to that of Tsou and Smith (1990), but different from that of Tracton (1990) who showed that the interaction component was clearly dominant. Following and expanding on the suggestion of Tracton (1990), more case studies are being examined to determine if the relative importance the planetary-scale, synoptic-scale, and interaction components are dependent on season, flow regime character, or geographical location. Finally, a high correlation between the synoptic-scale 300 mb wind field and the total interaction height tendencies was found.

7. Acknowledgments

The authors would like to thank co-workers Marty Rausch and Don Rolfson for their computer programming assistance and for their contributions during discussions. Also, we would like to thank Mike Seablom at the Goddard Laboratory for Atmospheres in Greenbelt, Maryland for his assistance in acquiring the data used for this study. Finally, the authors acknowledge the support of the National Aeronautics and Space Administration through NASA grant # NAG8-915.

REFERENCES

Agayan, G. M. and Mokhov, I. I. 1989. Quasistationary autumn regimes of the Northern Hemisphere atmosphere in FGGE. *Atms. Oc. Pys.* **25**, 1150–1156.

Alberta, T. L., Colucci, S. J. and Davenport, J. C. 1991. Rapid 500 mb cyclogenesis and anticyclogenesis. *Mon. Wea. Rev.* **119**, 1186–1204.

Austin, J. F. 1980. The blocking of middle latitude westerly winds by planetary waves. *Q. J. Roy. Meteor. Soc.* **106**, 327–350.

Baker, W. E., Bloom, S. C., Wollen, J. S., Nestler, M. S., Brin, E., Schlatter, T. W. and Branstator, G. W. 1987. Experiments with a three-dimensional statistical objective analysis scheme using FGGE data. *Mon. Wea. Rev.* **115**, 272–296.

Charney, J. G. and DeVore, J. G. 1979. Multiple flow equilibria in the atmosphere and blocking. *J. Atmos. Sci.* **36**, 1205–1216.

Colucci, S. J. 1985. Explosive cyclogenesis and large-scale circulation changes: Implications for atmospheric blocking. *J. Atmos. Sci.* **42**, 2701–2717.

Colucci, S. J. 1987. Comparative diagnosis of blocking versus non-blocking planetary circulation changes during synoptic scale cyclogenesis. *J. Atmos. Sci.* **44**, 124–139.

Dole, R. M. 1986. The life cycles of persistent anomalies and blocking over the North Pacific. *Adv. Geophys.* **29**, 31–70.

Fosdick, E. K. and Smith, P. J. 1991. Latent heat release in an extratropical cyclone that developed explosively over the southeastern United States. *Mon. Wea. Rev.* **119**, 193–207.

Frederiksen, J. S. 1982. A unified 3-D instability theory of the onset of blocking and cyclogenesis. *Mon. Wea. Rev.* **110**, 969–982.

Haltiner, G. J. and Williams, R. T. 1980. *Numerical prediction and dynamic meteorology*. New York: John Wiley & Sons, 478 pp.

Hansen, A. R. and Chen, T.-C. 1982. A spectral energetics analysis of atmospheric blocking. *Mon. Wea. Rev.* **110**, 1146–1165.

Harshvardhan, Davies, R., Randall, D. A. and Corsetti, T. G. 1987. A fast radiation parameterization for atmospheric circulation models. *J. Geophys. Res.* **92**, 1009–1016.

Illari, L. 1984. A diagnostic study of the potential vorticity in a warm blocking anticyclone. *J. Atmos. Sci.* **41**, 3518–3525.

Konrad, C. E. and Colucci, S. J. 1988. Synoptic climatology of 500 mb circulation changes during explosive cyclogenesis. *Mon. Wea. Rev.* **116**, 1431–1443.

Krishnamurti, T. N. 1968. A diagnostic balance model for studies of weather systems of low and high latitudes, Rossby numbers less than one. *Mon. Wea. Rev.* **96**, 518–530.

Lejenas, H. and Okland, H. 1983. Characteristics of Northern Hemisphere blocking as determined from a long time series of observational data. *Tellus* **35A**, 350–362.

Lejenas, H. and Madden, R. A. 1992. Traveling planetary-scale waves and blocking. *Mon. Wea. Rev.* **120**, 2821–2830.

Lupo, A. R., Smith, P. J. and Zwack, P. 1992. A diagnosis of the explosive development of two extratropical cyclones. *Mon. Wea. Rev.* **120**, 1490–1523.

Lupo, A. R. and Smith, P. J. 1995. Climatological features of blocking anticyclones in the Northern Hemisphere. *Tellus* **47A**, in press.

Maddox, R. A. 1980. An objective technique for separating macroscale and mesoscale features in meteorological data. *Mon. Wea. Rev.* **108**, 1108–1121.

McWilliams, J. C. 1980. An application of equivalent modons to atmospheric blocking. *Dyn. Atmos. Oc.* **5**, 43–66.

Mokhov, I. I. 1993. Diagnostics of the climate systems structure. *Gidrometeoizdat* (in Russian). St. Petersburg, 272 pp.

Mullen, S. L. 1987. Transient eddy forcing and blocking flows. *J. Atmos. Sci.* **44**, 3–22.

Petterssen, S. 1956. *Weather analysis and forecasting*, vol. I, 2nd edition, McGraw-Hill, 428 pp.

Rex, D. F. 1950. Blocking action in the middle troposphere and its effect on regional climate (II). The climatology of blocking action. *Tellus* **2**, 275–301.

Rex, D. F. 1951. Blocking action in the middle troposphere and its effect upon regional climate (I). *Tellus* **3**, 196–211.

Rodgers, E. and Bosart, L. F. 1991. A daignostic study of two intense oceanic cyclones. *Mon. Wea. Rev.* **119**, 965–996.

Sasamori, T. 1968. The radiative cooling calculation for application to general circulation experiments. *J. Appl. Meteor.* **7**, 721–729.

Schubert, S. D., Rood, R. D. and Pfaendtner, J. 1993. An assimilated dataset for Earth science applications. *Bull. Amer. Met. Soc.* **74**, 2331–2342.

Shapiro, R. 1970. Smoothing, filtering, and boundary effects. *Rev. Geophys.* **8**, 359–387.

Shutts, G. J. 1983. The propagation of eddies in diffluent jetstreams: Eddy vorticity forcings of blocking flow fields. *Q. J. Roy. Meteor. Soc.* **109**, 737–761.

Shutts, G. J. 1986. A case study of eddy forcing during an Atlantic blocking episode. *Adv. Geophys.* **29**, 135–161.

Simmons, A. J. 1986. Numerical prediction: Some results from operational forecasting at ECMWF. *Adv. Geophys.* **29**, 305–338.

Sperenza, A. 1986. Deterministic and Statistical properties of Northern Hemisphere middle latitude circulation. *Adv. Geophys.* **29**, 199–226.

Tibaldi, S. and Molteni, F. 1990. On the operational predictablity of blocking. *Tellus* **42A**, 343–365.

Tibaldi, S., Ruti, P., Tosi, E. and Maruca, M. 1993. Operational predictability of winter blocking: An ECMWF update. *Proc. ECMWF Seminars on Validation of forecasts and large-scale simulations over Europe*. ECMWF, Reading, Berkshire, UK.

Tibaldi, S., Tosi, E., Navarra, A. and Pedulli, L. 1994. Northern and Southern Hemisphere seasonal variability of blocking frequency and predictability. *Mon. Wea. Rev.* **122**, 1971–2003.

Tracton, M. S. 1990. Predictability and its relationship to scale interaction processes in blocking. *Mon. Wea. Rev.* **118**, 1666–1695.

Triedl, R. A., Birch, E. C. and Sajecki, P. 1981. Blocking action in the Northern Hemisphere: A climatological Study. *Atmos.-Oc.* **19**, 1–23.

Tsou, C.-H. and Smith, P. J. 1990. The role of synoptic/planetary-scale interactions during the development of a blocking anticyclone. *Tellus* **42A**, 174–193.

Tung, K. K. and Lindzen, R. S. 1979. A theory of stationary long waves, part I: A simple theory of blocking. *Mon. Wea. Rev.* **107**, 714–734.

Tung, K. K. and Lindzen, R. S. 1979. A theory of stationary long waves, part II: Resonant Rossby waves in the presence of realistic vertical shear. *Mon. Wea. Rev.* **107**, 735–750.

Tung, K. K. 1979. A theory of stationary long waves, part III: Quasi-normal modes in a singular wave guide. *Mon. Wea. Rev.* **107**, 751–774.

Zwack, P. and Okossi, B. 1986. A new method for solving the quasi-geostrophic omega equation by incorporating surface pressure tendency data. *Mon. Wea. Rev.* **114**, 655–666.